48 *Biochemistry* **2011,** *50,* 48–62
DOI: 10.1021/bi101594a

BIOCHEMISTRY
including biophysical chemistry & molecular biology
Article

NMR Reveals a Different Mode of Binding of the Stam2 VHS Domain to Ubiquitin and Diubiquitin[†,‡]

Anja Lange,[§] Daniela Hoeller,[∥] Hans Wienk,[⊥] Olivier Marcillat,[#] Jean-Marc Lancelin,[§] and Olivier Walker*[,§]

[§]*Université de Lyon, UMR-CNRS 5180 Sciences Analytiques, 69622 Villeurbanne, France,* [∥]*Division of Medical Biochemistry, Innsbruck Medical University, Biocenter, Fritz-Pregl-Strasse 3, 6020 Innsbruck, Austria,* [⊥]*Bijvoet Center for Biomolecular Research, NMR Spectroscopy, Utrecht University, Padualaan 8, 3584 CH Utrecht, The Netherlands, and* [#]*Institut de Chimie et Biochimie Moléculaires et Supramoléculaires, UMR-CNRS 5246, IMBL, Université Claude Bernard Lyon 1, 43, bd. du 11 Novembre 1918, 69622 Villeurbanne, France*

Received October 1, 2010; Revised Manuscript Received November 30, 2010

ABSTRACT: The VHS domain of the Stam2 protein is a ubiquitin binding domain involved in the recognition of ubiquitinated proteins committed to lysosomal degradation. Among all VHS domains, the VHS domain of Stam proteins is the strongest binder to monoubiqiuitin and exhibits preferences for K63-linked chains. In the present paper, we report the solution NMR structure of the Stam2-VHS domain in complex with monoubiquitin by means of chemical shift perturbations, spin relaxation, and paramagnetic relaxation enhancements. We also characterize the interaction of Stam2-VHS with K48- and K63-linked diubiquitin chains and report the first evidence that VHS binds differently to these two chains. Our data reveal that VHS enters the hydrophobic pocket of K48-linked diubiquitin and binds the two ubiquitin subunits with different affinities. In contrast, VHS interacts with K63-linked diubiquitin in a mode similar to its interaction with monoubiquitin. We also suggest possible structural models for both K48- and K63-linked diubiquitin in interaction with VHS. Our results, which demonstrate a different mode of binding of VHS for K48- and K63-linked diubiquitin, may explain the preference of VHS for K63- over K48-linked diubiquitin chains and monoubiquitin.

Ubiquitination is a core biological process which signals many cellular events and seals the fate of many proteins. This process is achieved by the covalent attachment of the C-terminal Gly76 of ubiquitin (Ub),[1] a small 76 amino acid protein, to a lysine residue of a target protein. Proteins can be modified by the attachment of Ub on one (monoubiquitination) (*1*) or several lysines (multimonoubiquitination) (*2*), as well as by the attachment of polyubiquitin chains (polyUb) (*3*). Ub harbors seven lysines which represent potential ligation points for the attachment of another Ub. Interestingly, depending on the type of ubiquitination, target proteins are committed to different pathways. Moreover, the outcome of polyubiquitination seems to rely on the structural assembly of polyUb chains. For instance, K48-linked polyUb is a unique signal for proteolysis and adopts a compact and closed conformation where the functionally important residues Leu8, Ile44, and Val70 are sequestered at the Ub/Ub interface (*4*−*7*). By contrast, K63-linked polyUb is involved in several nonproteolytic cellular signaling pathways (*8*−*11*) and adopts an elongated structure (*12*−*15*). Although monoubiquitination is involved in the endocytic process in yeast and mammalian cells (*1*, *16*, *17*), recent advances in the field suggest that multimonoubiquitination or K63-linked polyubiquitination is playing a major role in the multivesicular body (MVB) pathway (*18*, *19*). For instance, K63-linked ubiquitination of some cargoes like CPS and Gap1 (*20*) is required for their efficient sorting into the MVB pathway while only monoubiquitination is required for the sorting of Sna3 (*21*). K48-linked polyUb can also lead to lysosomal delivery but with a lower efficiency than K63-linked polyUb (*22*). One fundamental biological question raised is "Why are K63-linked chains favored in sorting cargoes to the MVB pathway?" One hypothesis is that K63-linked polyUb chains increase the local Ub concentration and favor avid binding. A second possibility is that K63-linked chains constitute a particular signal by exhibiting a different linker conformation for instance. Answering these questions requires a deeper understanding of the mechanistic and structural events that rule endocytic sorting.

The machinery responsible for committing ubiquitinated cargoes for lysosomal degradation is known as the ESCRT system (*23*−*25*). The upstream component, ESCRT-0, is constituted by the Hrs/Stam complex in mammalian cells (Vps27/Hse1 complex in yeast). Recognition of ubiquitinated cargoes is achieved by modular motifs called ubiquitin binding domains (UBDs) (*26*−*28*) which have been found to function cooperatively (*29*). Altogether, the Stam and Hrs heterodimers possess five UBDs among which the VHS domain has been found to be a key player in cargo sorting for lysosomal degradation (*30*, *31*). The VHS domains have been found to bind monoubiquitin (monoUb) with different

[†]This work was partially performed at the Utrecht NMR Facility funded by the European Union (EU-NMR; Grant RII3-026145). The eNMR project is supported by a European FP7 e-Infrastructure grant, contract 213010 (www.enmr.eu). A.L. is the recipient of a MENRT fellowship.

[‡]PDB accession codes: Stam2 VHS (1X5B); ubiquitin (1D3Z); monoUb/Stam1 VHS complex (3LDZ); monoUb/Stam2 VHS complex (2L0T); K63-Ub_2 (2JF5); K48-Ub_2 (1AAR).

*To whom correspondence should be addressed. Phone: +33.4.72.43.18.27. Fax: +33.4.72.43.13.95. E-mail: olivier.walker@univ-lyon1.fr.

[1]Abbreviations: CSP, chemical shift perturbations; PRE, paramagnetic relaxation enhancement; Ub, ubiquitin; monoUb, monoubiquitin; polyUb, polyubiquitin; SL, spin label; MTSL, (1-oxy-2,2,5,5-tetramethyl-3-pyrroline-3-methyl) methanethiosulfonate; K48-Ub2, K48-linked diubiquitin; K63-Ub2, K63-linked diubiquitin.

 Published on Web 12/01/2010

affinities whereas the VHS domain of Stam1 shows a preference for K63- over K48-linked diubiquitin chains and monoUb (*32*, *33*). These results obviously raised several questions and need further development. For instance, "Why do various VHS domains exhibit different affinities for monoUb?" and "Why do some VHS domains show a preference for K63-linked diubiquitin (K63-Ub_2) over K48-linked diubiquitin (K48-Ub_2) and monoUb?" In an attempt to answer these crucial questions, we report the solution structure of the monoUb/Stam2-VHS complex by using chemical shift perturbations (CSPs), spin relaxation, and a paramagnetic probe to constrain the structure. We show that the monoUb/VHS interaction exhibits 1:1 stoichiometry and is mainly hydrophobic although some electrostatic contacts are involved. Moreover, we examine the interaction of VHS with K48- and K63-Ub_2 chains in order to understand the structural details that account for the selective preference of VHS toward K63-Ub_2 chains. We show that the VHS/K48-Ub2 and VHS/K63-Ub2 complexes exhibit a different mode of binding and are associated with different stoichiometries.

MATERIALS AND METHODS

Expression and Purification of VHS. The human Stam2 VHS domain (1−149) (including its mutants W33A, D32A, and N82A) in pETEM-60 (Novagen) was expressed N-terminally fused to NusA and a hexahistidine tag (His_6 tag). For overexpression the constructs were transformed into *Escherichia coli* BL21 (DE3). Cells were grown either in LB medium or for uniform isotopic labeling in M9 medium supplemented with 1 mM $MgSO_4$, 1 mM $CaCl_2$, 4 g/L D-glucose, 6 μg/L thiamin, and 1 g/L $^{15}NH_4Cl$ as sole nitrogen source. For ^{13}C-labeled protein $^{12}C_6$-D-glucose was exchanged for 4 g/L $^{13}C_6$-D-glucose. The cells were grown until OD_{600} reached 0.8 and induced by addition of 1 mM IPTG. Induction was performed for 5 h at 30 °C. The cells were lysed in 50 mM Tris-HCl, pH 7.8, 250 mM NaCl, 10 mM imidazole, 5% (v/v) glycerol, and 5 mM β-Me. The clarified cell lysate was loaded on a 5 mL HisTrap FF column (GE Healthcare) equilibrated with 50 mM Tris-HCl, pH 7.8, 250 mM NaCl, 10 mM imidazole, 1% (v/v) glycerol, and 5 mM β-Me. The bound protein was eluted by applying an imidazole gradient. NusA and His_6 tag were removed by cleavage with tobacco etch virus protease (TEV) at 4 °C overnight. VHS was separated from NusA-His_6 by size exclusion chromatography using a Sephacryl 100 16/60 column (GE Healthcare) and then exchanged in 20 mM sodium phosphate buffer, pH 6.8.

TEV was expressed N-terminally fused with MBP-TEV cleavage site−His_6 tag. During expression the fusion protein underwent autocleavage leaving His_6-tagged TEV. The TEV construct was transformed in *E. coli* BL21 (DE3), and cells were grown in LB medium at 37 °C until OD_{600} reached ≈1 and induced at 20 °C overnight. For the purification of TEV, a HisTrap FF column (GE Healthcare) was used. For storage, TEV was brought to 50% glycerol and frozen at −80 °C.

Recombinant ubiquitins wt Ub, Ub (K48C), Ub (T12C), and segmentally isotope-labeled Ub_2s linked via K48 (K48-Ub_2) or K63 (K63-Ub_2) were prepared as described (*5*, *13*).

NMR Experiments. The ensemble of NMR data was acquired at 288 K where the NMR samples were exchanged into a buffer containing 20 mM sodium phosphate at pH 6.8, 10% D_2O, 0.02% (w/v) NaN_3, and either [NaCl] = 100 mM or [NaCl] = 0 mM. Assignment and relaxation experiments of the VHS sample have been acquired on a Bruker Avance 900 and 600 MHz equipped with triple resonance probes (large scale NMR facility Utrecht) whereas titration experiments have been carried out on a Varian Inova Unity 600 equipped with a triple resonance probe.

VHS Resonance Assignment and Structure. The backbone resonance assignment were obtained by means of the combination of the following experiments: [^{15}N,^{1}H]-HSQC, CBCA(CO)NH, HNCA, HNCACB, and 3D NOESY-[^{15}N,^{1}H]-HSQC. Experiments were processed with NMRpipe (*34*) and analyzed with SPARKY (*35*) starting with the assignment list provided by the Riken Institute (structure determination of the Stam2 VHS, PDB code 1X5B). Based on amide ^{1}H, ^{15}N, C_α, and C_β carbon chemical shifts, the presence, position, and length of secondary structure elements were predicted with TALOS (*36*). CS-ROSETTA (*37*, *38*) was then used and predicted the eight α helices of the VHS domain, allowing us to use the solution NMR VHS structure previously released (PDB code 1X5B). Compared to the sequence corresponding to the Stam2 VHS released under PDB code 1X5B, our VHS domain contains the extension GAMG instead of GSSGSS in the N-terminus and also does not contain the extension TSGPSSG in the C-terminus. Thus, the use of the current solution NMR structure (PDB code 1X5B) is justified by the fact that no interactions between the N- or C-terminus of VHS and monoUb or Ub_2 were detected.

Relaxation Measurement and Analysis. Relaxation experiments included ^{15}N longitudinal (R_1), transverse (R_2) relaxation, and the $^{15}N-^{1}H$ cross-relaxation rates via steady-state $^{15}N\{^{1}H\}$ NOE were obtained from experiments previously described (*39*). Experiments have been recorded with spectral widths of 2000 Hz in the ^{15}N dimension and 9600 Hz in the ^{1}H dimension. For the R_1 measurements, we used 10 relaxation delays: 4, 20, 40, 80 (twice), 240, 480, 800 (twice), 1200, 1600, and 2000 ms with a recycling delay of 5 s. The R_2 measurements were performed with a transverse relaxation period of 4, 12, 24, 32 (twice), 48, 56, 80, 120 (twice), 160, and 200 ms with a relaxation delay of 5 s. For $^{15}N\{^{1}H\}$ nuclear Overhauser effect experiments, 2D spectra were recorded with and without presaturation of amide protons (*40*). The recycle delay was set to 6 s in order to allow the bulk water magnetization to return as closely as possible to its equilibrium value. All NMR data were processed with NMRpipe (*34*) and analyzed with NMRViewJ (*41*). The ^{15}N relaxation rates and heteronuclear NOEs were analyzed using ROTDIF (*42*) by only considering residues which belong to the well-defined core of the protein.

NMR Titration Studies. Interaction surfaces on monoUb, Ub_2, and VHS were characterized by means of chemical shift perturbation where a series of $^{1}H-^{15}N$ HSQC spectra were recorded for a protein while adding small volumes of concentrated binding partner. To avoid aggregation of one of the proteins, we started from a ^{15}N-labeled protein (P) concentration of 250 μM and added increasing volumes of a concentrated stock of the nonlabeled ligand protein (L) until reaching a plateau. To derive the corresponding binding constant, CSPs were analyzed by calculating the combined amide chemical shift perturbation ($\Delta\delta$) as $\Delta\delta = [((\Delta\delta_H)^2 + (\Delta\delta_N/5)^2)/2]^{1/2}$. Different binding models have been tested for the different titration curves (*13*, *43*). Considering a 1:1 stoichiometry allows one VHS molecule bound per Ub_2 or monoUb and assumes that one VHS can bind to either of the two Ub domains but not both. The perturbations observed on VHS do not discriminate between the two Ub domains so that the observed chemical shift perturbation is a weighted average between the two extreme values corresponding to the free

($\Delta\delta = 0$) and ligand-bound state ($\Delta\delta = \Delta\delta_{LB}$):

$$\Delta\delta = \Delta\delta_{LB}([L_0] + [P_0] + K_d - \sqrt{([L_0] + [P_0] + K_d)^2 - 4[L_0][P_0]})/2[P_0] \quad (1)$$

where $[P_0]$ and $[L_0]$ are the total molar concentrations of VHS and Ub_2, respectively. For the 2:1 binding model, we have

$$\Delta\delta = \Delta\delta_{LB}(2[L_0] + [P_0] + K_d - \sqrt{(2[L_0] + [P_0] + K_d)^2 - 8[L_0][P_0]})/2[P_0] \quad (2)$$

For measurements on the distal or the proximal domains, the 1:1 model gives

$$\Delta\delta = \Delta\delta_{LB}\left([L_0] + [P_0] + \frac{1}{2}K_d - \sqrt{\left([L_0] + [P_0] + \frac{1}{2}K_d\right)^2 - 4[L_0][P_0]}\right)/4[P_0] \quad (3)$$

where $[P_0]$ and $[L_0]$ are the total molar concentrations of Ub_2 and VHS, respectively. For the 2:1 model, we used

$$\Delta\delta = \Delta\delta_{LB}([L_0] + 2[P_0] + K_d - \sqrt{([L_0] + 2[P_0] + K_d)^2 - 8[L_0][P_0]})/4[P_0] \quad (4)$$

The dissociation constant K_d and $\Delta\delta_{LB}$ were fitted with nonlinear regression by using an in-house Matlab (The MathWorks, Inc.) based program. Errors were estimated by sampling 100 initial guesses, assuming 10% error on the protein and ligand concentrations.

NMR Line Shape Analysis. The dissociation and association rates have been investigated by means of line shape analysis with the "LINESHAPEKIN" software (*44*) (http://lineshapekin.net/). Residues undergoing significant shifts along the titration experiments were used to extract the dissociation rate (k_{off}) and a scaling factor whereas the dissociation constant (K_d) was used as an input parameter. All chosen residues were simultaneously fitted using a global, two-state model.

MonoUb/VHS Docking. The structure of the monoUb/VHS complex has been calculated with the HADDOCK2.0 program (*45*, *46*). Ten NMR structures of monoUb and VHS have been used (PDB codes 1D3Z and 1X5B) as starting points. To take into account paramagnetic relaxation enhancement (PRE) data, a cysteine residue and MTSL have been introduced in silico at positions 48 and 12 in the monoUb structure. The PRE intermolecular distances were introduced as distances separating the oxygen atom of MTSL and a given amide proton of VHS (see Supporting Information Table ST1) with an additional upper and lower bound distance of 4 Å. In addition, CSPs were introduced to define ambiguous interaction restraints (AIRs). Active residues were defined as those having CSPs above 0.05 and 0.1 ppm for VHS and monoUb, respectively, and a relative residue accessible surface area larger than 50% for side chains or backbone atoms. Passive residues were identified as residues close to active residues. Flexible segments were defined as stretches of active and passive residues plus one sequential residue. To provide orientational restraints, relaxation data were included in the rigid body minimization as a R_2/R_1 ratio for both proteins in the bound state. The rotational diffusion tensor was allowed to rotate freely during the two first step of structure calculation (randomization of orientation and semiflexible simulated annealing), whereas it was kept fixed during the last step (water refinement). Finally, the structure calculation was done with the standard three step refinement found in HADDOCK with (i) a rigid body energy minimization generating 3000 structures, (ii) semiflexible refinement using the best 300 structures, and (iii) final refinement in water. The 300 final solutions were ranked according to the Haddock score, defined as $1.0E_{vdw} + 0.2E_{elec} + 0.1E_{AIR} + 1.0E_{desolv}$. Thus, they were clustered based on a backbone rmsd of 5.5 Å, and the 10 best structures of the best cluster in terms of Haddock score were retained for analysis. All docking calculations have been carried out on the e-NMR web portal.

Site-Directed Spin Labeling and PRE Analysis. MTSL compound was attached to two Ub mutants or the proximal domain of Ub_2 mutants (K48C and T12C) through the side chain of cysteine as described previously (*47*). The PRE effect was measured as a ratio of signal intensities in the oxidized (paramagnetic) and reduced (diamagnetic) state (*48*):

$$I_{ox}/I_{red} = \exp(-t\Delta R_{2para}) \quad (5)$$

where t is the total experimental time when the amide proton magnetization is in the transverse plane and undergoing paramagnetic relaxation.

The oxidized spectrum was obtained by directly looking at Ub in the case where MTSL was attached to ^{15}N labeled Ub or by mixing a MTSL attached to unlabeled Ub or Ub_2 to ^{15}N-VHS. The reduced spectrum is obtained by mixing 3 molar equiv of ascorbic acid with the oxidized sample. The PRE data were converted to distances between the unpaired electron and the amide proton spins according to the equations previously established (*48*−*51*):

$$\Delta R_{2para} = \frac{1}{20}\gamma_H^2 g_e^2 \beta_e^2 \left(4\tau_c + \frac{3\tau_c}{1+\omega^2\tau_c^2}\right)\left\langle\frac{1}{r^6}\right\rangle \quad \text{where } \Delta R_{2para} = R_{2ox} - R_{2red} \quad (6)$$

τ_c is the rotational correlation time of the molecule, γ_H and ω_H are the H gyromagnetic ratio and resonance frequency, g_e is the electronic g-factor, and β_e is the Bohr magneton. The angular brackets represent the averaging between the two populated structures in states A and B corresponding to distances r_A and r_B. If the exchange between the two states occurs on a much faster time scale than the spin relaxation, then

$$\left\langle\frac{1}{r^6}\right\rangle = \frac{p_A}{r_A^6} + \frac{p_B}{r_B^6}$$

where p_A and p_B represent the different populations describing states A and B whereas r_A and r_B represent the distance between the unpaired electron and a given amide proton of the ^{15}N-labeled sample in state A or B. For the monoUb/VHS interaction, p_B has been set to 0. For a two-state case, a grid search has been generated by sampling p_A between 0 and 1. The value of p_A which gives the lowest target function has been retained as well as the position of the two centers (hence six coordinates) for the current value of p_A.

For the residues whose resonance disappeared in the oxidized state, their intensity was estimated from the noise level in the spectrum. For the monoUb/VHS complex τ_c was derived from spin relaxation data analysis. For the Ub_2/VHS complex τ_c was estimated by assuming a linear dependence of τ_c with the molecular

weight. R_{2dia} was estimated from the transverse relaxation rate of monoUb bound to VHS, Ub_2 bound to VHS, or monoUb in the free state. The position of the unpaired electron was derived after a global fit of the observed PREs and by selecting residues in the well-structured part of the protein. The fit was carried out by using the SLfit program (*51*) modified to take into account two paramagnetic centers. Distances were calculated between the position of the paramagnetic center and the position of a given amide proton.

Protein Data Bank Accession Number. Atom coordinates of the monoUb/VHS complex have been deposited to the Protein Data Bank with accession number 2L0T.

RESULTS

Mapping the Ub/VHS Interface. We used chemical shift perturbations (CSPs) (*52*−*54*) to map the interaction between the VHS domain of Stam2 and monoUb. Based on CSPs, our results suggest a highly specific interaction surface between VHS and monoUb mainly mediated by hydrophobic contacts. Chemical shift perturbations were observed on the VHS ^{1}H,^{15}N-HSQC spectrum upon addition of ubiquitin (see Supporting Information Figure SF1). The largest perturbations cluster in a contiguous patch around helix α2 and α4 affecting residues Thr29 to Asp41 and Thr74 to Asn82 (Figure 1a−c). VHS exhibits the largest CSPs on the hydrophobic residue Trp33 and acidic side chain residues Asp32 and Asn82. From the monoUb side, chemical shift perturbations mainly involve the hydrophobic residues Ile13, Ile44, Ala46, Leu50, and Val70 (Figure 1d−f and Supporting Information Figure SF2) located in three structural regions corresponding to the hydrophobic patch involved in most of the monoUb/UBDs interactions (*26*, *27*). Furthermore, Gly47, Gln49, and Leu71 disappeared during the titration whereas Leu8, Leu50, Arg72, and Val70 experienced strong signal attenuation by the end of titration suggesting intermediate exchange. The analysis of the CSP data of ^{15}N-VHS upon addition of monoUb yields a dissociation constant (K_d) of 64 ± 8 μM whereas we derived a K_d of 54 ± 6 μM after analysis of the ^{15}N-monoUb titration curve (Figure 1b,e, Table 1). This value is within the same order of magnitude of previous dissociation constants determined by Hond et al. on Stam1 (*33*). The kinetics of the interaction between monoUb and VHS was determined with the assumption of 1:1 binding and by use of line shape analysis for ^{1}H,^{15}N-HSQC NMR spectra acquired during the titration of unlabeled VHS into ^{15}N-monoUb, to yield estimates of (∼1.3 ± 0.1) × 10^8 M^{-1} s^{-1} and 7040 ± 350 s^{-1} for k_{on} and k_{off}, respectively (Supporting Information Figure SF3).

Stoichiometry of the MonoUb/VHS Complex. Analysis of spin relaxation parameters was used, in conjunction with CSPs, to determine the stoichiometry of the monoUb/VHS complex. ^{15}N R_1 and ^{15}N R_2 relaxation rates report on the overall tumbling (hence the molecular mass) of the molecule under investigation (*50*). ^{15}N longitudinal relaxation rates (R_1) and ^{15}N transversal relaxation rates (R_2) as well as heteronuclear NOE have been measured for the free form of ^{15}N-VHS and ^{15}N-monoUb as well as for ^{15}N-VHS/^{14}N-monoUb and ^{15}N-monoUb/^{14}N-VHS samples (Figure 2). Measurements for the target protein in the complex were carried out under saturating conditions for both VHS and monoUb. For monoUb, the average R_1 for residues in secondary structure elements decreases from 1860 ± 74 ms^{-1} for the free form to 972 ± 110 ms^{-1} for the complexed form. The R_1 values in the bound form for both monoUb and VHS correspond to a molecular mass ranging from 20.6 to 27.5 kDa, which are in good agreement with the expected molecular mass of 25.4 kDa for a 1:1 VHS/Ub complex (Supporting Information Figure SF4). The measured R_2 for monoUb and diubiquitin (Ub_2) is 7.3 ± 0.4 and 12.6 ± 0.5 s^{-1}, respectively, hence roughly proportional to the molecular mass. Both monoUb and VHS sense practically the same R_2 in the bound state: R_2(bound monoUb) = 22.5 ± 1.8 s^{-1} and R_2(bound VHS) = 23.4 ± 1.7 s^{-1}, whereas VHS exhibits a R_2 value of 17 ± 0.8 s^{-1} in the free state. The 1:1 complex stoichiometry is also supported by the correlation time which leads to a direct measurement of its molecular mass. The corresponding τ_c for the free monoUb is 5.6 ± 0.4 and 15.7 ± 1.4 ns for monoUb in the bound state, which corresponds to a roughly 3-fold increase. When VHS is binding monoUb, the overall tumbling time of VHS is 16.2 ± 1.3 ns.

Spin Relaxation as Orientational Constraints. Spin relaxation measurements report on the overall rotational diffusion and structure of molecules. This information can be used to orient the components of the monoUb/VHS complex with respect to each other (*50*) and also to drive molecular docking (*55*). Therefore, the relative orientation of VHS with respect to monoUb can be obtained by simply rotating their respective diffusion tensors so that they become collinear (*5*, *50*, *56*−*58*). The analysis of the relaxation data was performed by means of the ρ factor approach (*42*, *59*, *60*) implemented in Rotdif (*42*). The rotational diffusion tensor orientation was determined for each protein in the free form and in the complexed form. According to our statistical analysis (Supporting Information Table ST2), the axially symmetric model agrees with the experimental relaxation data for the free form of both monoUb and VHS where the orientation of the corresponding rotational diffusion tensor is given by α = 107 ± 10°, β = 156 ± 22° and α = 103 ± 18°, β = 99 ± 19° for monoUb and VHS, respectively. In contrast to these results, the fully anisotropic model prevails for the monoUb/VHS complex when derived from either monoUb or VHS relaxation data. This is also the case when the rotational diffusion tensor is derived by using the structure of the calculated complex. The alignment of individual rotational diffusion tensors for monoUb and VHS gives rise to four different solutions due to the absence of directionality for the rotational diffusion axes. Among these solutions, only two were retained based on observed chemical shift perturbations (Supporting Information Figure SF6).

Paramagnetic Spin Labeling Provides MonoUb/VHS Intermolecular Distances. While the rotational diffusion tensor for the monoUb/VHS complex can provide the relative orientation of each protein with respect to each other, intermolecular distance information is lacking. An accurate approach is the use of site-directed spin labeling to derive unambiguous long distance constraints and identify low populated structures (*61*−*63*). We used MTSL (1-oxy-2,2,5,5-tetramethyl-3-pyrroline-3-methyl) methanethiosulfonate as a paramagnetic species (*64*). The paramagnetic tag causes strong signal attenuation to nuclei that are close in space via the paramagnetic relaxation enhancement (PRE) effect. To check the attachment of the SL to monoUb, we attached the SL to two mutated ^{15}N-monoUb (K48C and T12C). The analysis of the magnitude of the PREs allowed us to reconstruct the position of the SL (see Supporting Information Figure SF5). On either the K48C or T12C mutant, the position of MTSL derived from the analysis of PRE data is in relatively good agreement with the expected position of a MTSL radical mutated "in silico" at position Cys48 or Cys12 (see Supporting Information Figure SF5c,d). Nevertheless, one has to bear in mind that the processing of PRE data can only afford the time-averaged

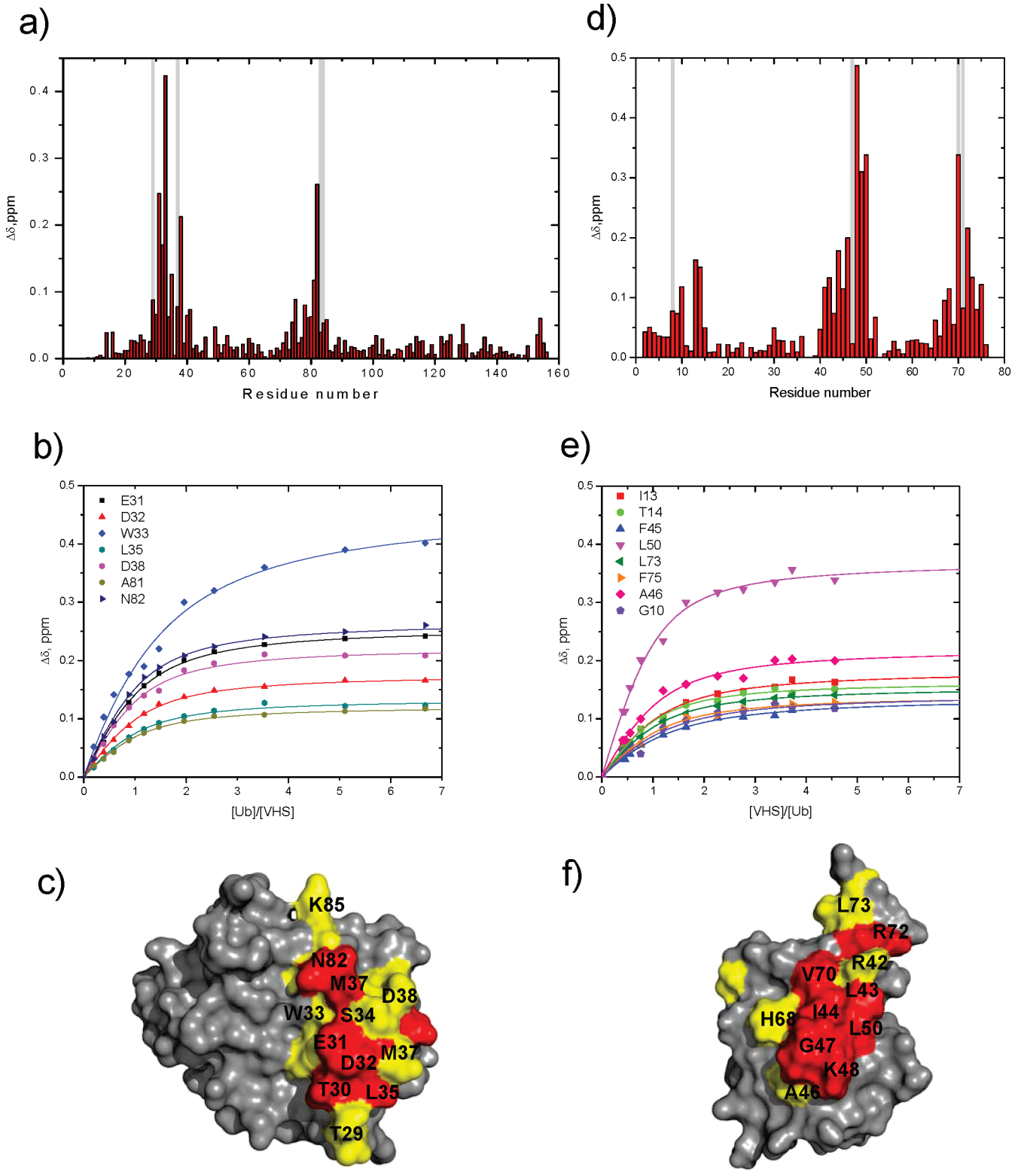

FIGURE 1: CSP mapping of the interaction between VHS and monoUb. CSPs in VHS (a) and monoUb (d) at the end point of titration as a function of residue number. Cross-peaks experiencing intermediate exchange in the $^{1}H,^{15}N$-HSQC spectrum are marked by gray bars. Titration curves on ^{15}N-VHS (b) and ^{15}N-monoUb (e) as a function of the molar ratio of the ligand and the ^{15}N-protein. Representation of the binding interface on VHS (c) and monoUb (f). Residues that exhibit significant shifts are colored red ($\Delta\delta > 0.1$) and yellow ($0.1 \geq \Delta\delta > 0.05$) for VHS whereas red and yellow residues indicate $\Delta\delta > 0.15$ and $0.15 \geq \Delta\delta > 0.1$, respectively, for monoUb.

position of the spin label (SL) due to its intrinsic flexibility. The distance between the reconstructed SL position and the α carbon of C48-monoUb or C12-monoUb is 10.8 and 10.2 Å, respectively, in good agreement with the theoretical distance of 9.2 Å between the oxygen of the MTSL molecule and the α carbon of C48-monoUb or C12-monoUb. Next, we observed PREs on ^{15}N-VHS in the presence of monoUb covalently attached to SL (Cys48 or Cys12). At this point, it is important to mention that the attachment of the spin label did not perturb the interaction between VHS and monoUb, as can be seen on Supporting

Information Figure SF6. It is worth emphasizing here that the decrease in signal intensity affects not only residues that exhibit strong chemical shift perturbations located around Glu31 and Asn82 (Figure 3a) but also residues flanking Met120. It is noteworthy that the observed PREs are in good agreement with the chemical shift perturbations. Indeed, the SL affects the same interface as the binding interface identified by CSPs. Additionally, when the T12C-monoUb mutant is used (Figure 3b), we observed attenuations occurring around residue Thr30 of VHS, indicating that Cys12 is mainly facing a region that encompasses residue Thr30 (α1/α2 loop). The derived distances indicate that the Lys48 of monoUb is approaching Asn82 of VHS at a distance of 8 Å whereas monoUb Thr12 is facing VHS Asp32 with a distance of 10 Å (Supporting Information Figure SF7). The distance between the reconstructed positions of the MTSL radical attached on C48 and C12 is 23.5 Å. As a comparison, we measured a distance 26.8 Å between the reconstructed position of the SL attached to C48 and C12 for PREs recorded from the ^{15}N-VHS side (Figure 3d).

Table 1: Summary of the Dissociation Constants Derived from NMR Titration Curves[a]

sample	K_d (μM) 0 mM NaCl	K_d (μM) 100 mM NaCl
^{15}N-VHS/monoUb	64 (8)	156 (14)
^{15}N-monoUb/VHS	54 (6)	166 (12)
^{15}N-VHS D32A/monoUb	362 (22)	
^{15}N-VHS W33A/monoUb	4100 (400)	
^{15}N-K48-Ub$_2$ distal/VHS[b]	16 (6)	
^{15}N-K48-Ub$_2$ proximal/VHS[b]	101 (12)	
^{15}N-VHS/K48-Ub$_2$[c]	43 (8)	
^{15}N-K63-Ub$_2$ distal/VHS[d]	34 (6)	
^{15}N-K63-Ub$_2$ proximal/VHS[d]	45 (8)	
^{15}N-VHS/K63-Ub$_2$[e]	36 (8)	

[a]Errors are shown in parentheses. [b]K_d obtained with a 1:1 model (eq 3). The 2:1 model gave a higher value of the target function. [c]K_d obtained with a 1:1 model (eq 1). The 2:1 model gave a higher value of the target function [d]K_d obtained with a 2:1 model (eq 4). The 1:1 model gave a higher value of the target function. [e]K_d obtained with a 2:1 model (eq 2). The 1:1 model gave a higher value of the target function.

Furthermore, the reconstruction of the paramagnetic center allows us to discriminate from the two remaining models obtained from the alignment of the rotational diffusion tensors. The structure (c) from Supporting Information Figure SF8 is the one that exhibits the best agreement between (i) the position of the SL for C48-monoUb and ^{15}N-VHS + C48-monoUb and (ii) the position of the SL for C12-monoUb and ^{15}N-VHS + C12-monoUb.

Modeling the MonoUb/VHS Complex. The structure of the monoUb/VHS complex was modeled using molecular docking methods with NMR constraints (CNS) (*65*) and the Haddock2.0 program (*45*, *46*). As starting structures, we used the NMR structure of each individual protein (PDB code 1D3Z for monoUb (*66*) and 1X5B for VHS). To take into account the fact that the paramagnetic effect originates from the unpaired electron of the SL, cysteine residues and MTSL atoms were introduced "in silico" at positions 12 and 48 on monoUb. We included three different kinds of constraints to drive the docking (see Materials and Methods and Supporting Information Table ST1): (i) nine different distances derived from PREs were included as unambiguous distance constraints, (ii) chemical shift perturbations were included as ambiguous distances, and (iii) the rotational diffusion tensor measurements were included as R_2/R_1 ratios (*55*). It has to be pointed out here that we also modeled the monoUb/VHS complex by using 20 different distances derived from PRE data. Because the resulting structure did not differ from the one obtained with the nine most reliable distances, it has been decided to keep these constraints only. The resulting structures were subjected to clustering. Details of the docking results are summarized in Table 2 for the 10 best structures of the best cluster whereas the 10 best structures of the best cluster are presented in Figure 3c.

When dealing with the best structure of the best cluster, the measured distance between the reconstructed position of the SL attached to C12 and the amide proton of Asp32 (VHS) is 12.8 Å (11.2 Å estimated from PRE data; see Figure 3d and Supporting Information Figure SF7) whereas we measured a distance of 5.1 Å between the reconstructed position of MTSL attached to C48 and the amide proton of Asn82 (8.6 Å estimated from PRE data), thus showing a relatively good agreement between the

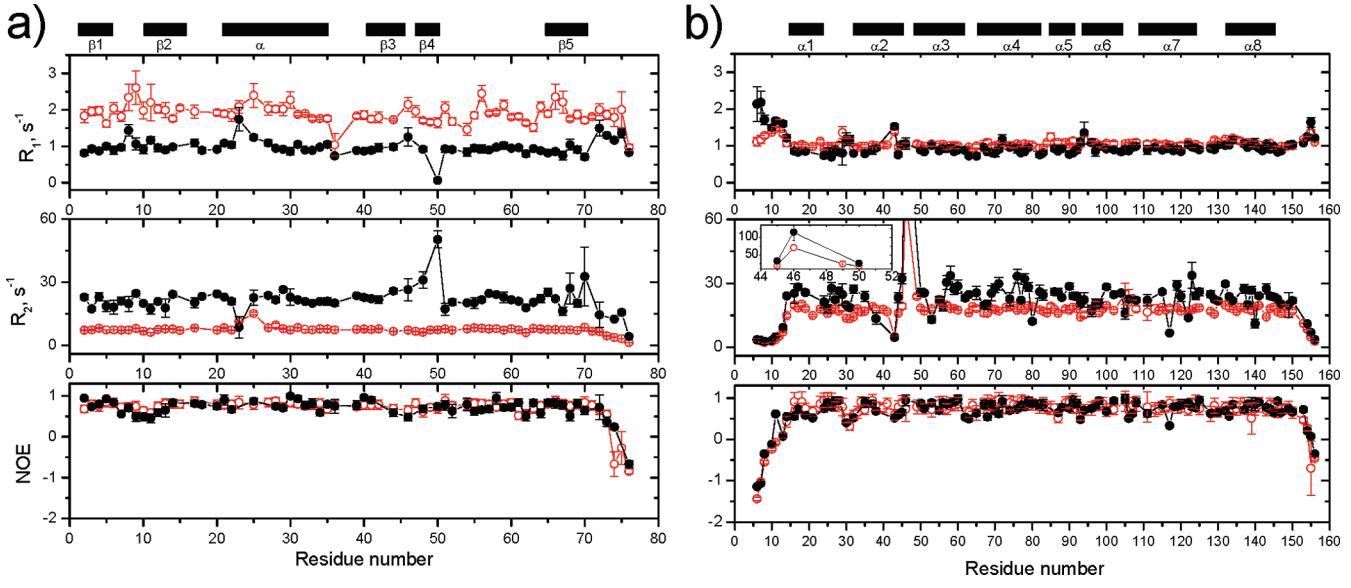

FIGURE 2: Relaxation parameters R_1, R_2, and heteronuclear NOE for both monoUb (a) and VHS (b) in the free (red open circles) and bound form (black plain circles). The relative shift of the different levels reflects the change in the overall molecular tumbling for each partner and hence their molecular mass upon complex formation.

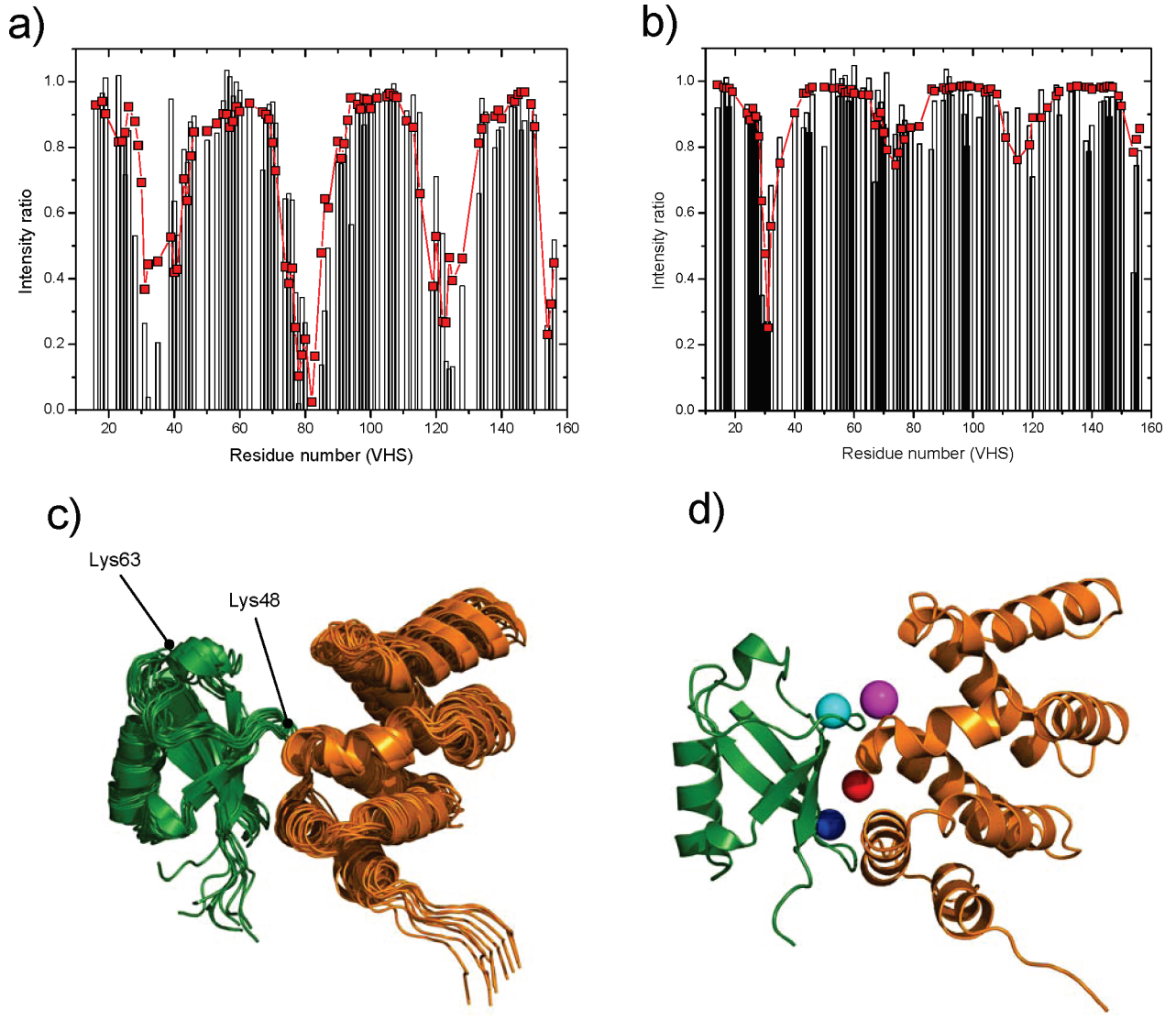

FIGURE 3: Analysis of the PRE data for SL-monoUb complexed with ^{15}N-VHS (a, b). (a) Experimental intensity ratio for SL-C48-monoUb + ^{15}N-VHS and (b) SL-C12-monoUb + ^{15}N-VHS is represented by black bars whereas the red line and symbols represent back-calculated PREs for the fitted SL position. (c) Cartoon representation of the structure of the monoUb/VHS complex obtained from Haddock docking showing the 10 best structures of the best cluster. MonoUb is colored green whereas VHS is colored orange. Positions of the reconstructed MTSL for both partners involved in the complex (d). The orientation of VHS with respect to monoUb is similar to the one seen in (c). The structure used for the representation is the best structure of the best cluster. The reconstructed SL position is shown as a sphere colored magenta for C48-monoUb, red for C12-monoUb, cyan for SL-C48-monoUb + ^{15}N-VHS, and blue for SL-C12-monoUb + ^{15}N-VHS. The distance between the magenta and cyan ball is 8.4 Å whereas we measured a distance of 5.4 Å between the blue and red ball.

distances estimated from PRE data and the final structure of the complex.

Hydrophobic and Electrostatic Interactions Contribute to the MonoUb/VHS Interaction. According to our docking results, VHS binds mainly monoUb through the α2 and α4 helices to a surface defined by the β3 and β4 strands of monoUb. The ubiquitin surface in contact with VHS involves a deep hydrophobic pocket and appears to be stabilized by intermolecular electrostatic interactions delimited by the turn region between α1 and α2 of VHS. Glu31, Asp32, and Asp41 are involved in electrostatic interactions with Lys6 and Arg72 of monoUb whereas several hydrogen bonds encompass the previous interaction (Supporting Information Figure SF9). To assess the contribution of electrostatic contacts, we derived the dissociation constant from other experimental conditions. Increasing the NaCl concentration from 0 to 100 mM increases the K_d (hence a lower binding) to 156 ± 14 μM from the VHS side and 166 ± 12 μM from monoUb side (Supporting Information Figure SF10, Table 1), whereas the overall shape of CSPs is not modified. This represents an average 2.5 times increase of the K_ds when the NaCl concentration increases from 0 to 100 mM and demonstrates that electrostatic interactions play a role in the monoUb/VHS interaction. To estimate the importance of the most shifted residues (i.e., Asp32, Trp33, and Asn82), we engineered three different ^{15}N-labeled VHS mutants, D32A, W33A, and N82A, where all three ^{1}H,^{15}N-HSQC spectra correspond to well-folded proteins. We followed chemical shift perturbations upon addition of monoUb (with [NaCl] = 0 mM) and observed a K_d of 362 ± 22 and 4.1 ± 0.4 mM for D32A and W33A, respectively (Table 1, Figure SF11) whereas addition of monoUb to N82A resulted in the precipitation of the sample. As judged by the results, the mutation of D32 and W33 gave rise to a 5 and 64 times increase of K_d, which potentially accounts for the importance of these highly conserved residues on VHS.

The Interaction of VHS with Diubiquitin Chains. To shed light on the binding of VHS with K48- and K63-linked diubiquitin

Table 2: Haddock Restraints as Well as Results of the Structure Calculation for the 10 Best Structures of the Best Cluster for the MonoUb/VHS Interaction

Haddock Restraints									
ambiguous restraints from CSPs			active				passive		
			11 (Ub)				8 (Ub)		
			11 (VHS)				4 (VHS)		
unambiguous distance restraints from PREs			9 (4 from C48; 5 from C12)						
DANI restraints			50						

Ub/VHS Complex Structure Calculation									
E_{inter}[a]	E_{vdW}	E_{elec}	E_{NOE}[b]	E_{DANI}[c]	BSA[d]	H_{bond}[e]	hydro[f]	score[g]	rmsd[h]
−413.4 (23.0)	−34.6 (5.4)	−378.8 (26.0)	9.0 (2.4)	54 (5)	1138 (102)	9.4 (1.0)	20 (2)	−72.0 (3.7)	1.54 (0.7)

Procheck Analysis	
residues in most favored region (%)	88.0
residues in additionally allowed region (%)	11.6
residues in generously allowed regions (%)	0.4
residues in disallowed regions (%)	0.0

[a]Intermolecular energy: sum of the van der Waals and electrostatic energies (kcal·mol^{-1}). [b]NOE energy: sum of the ambiguous and unambiguous energies (kcal·mol^{-1}). [c]DANI energy: *d*iffusion *ani*sotropy (relaxation data) energy (kcal·mol^{-1}). [d]Total buried surface area for Ub and VHS (Å^2). [e]Number of hydrogen bonds. [f]Number of hydrophobic contact. [g]Haddock score (arbitrary units). [h]Backbone rmsd calculated with respect to the lowest Haddock score structure.

chains (K48-Ub_2 and K63-Ub_2), we engineered segmentally ^{15}N-labeled Ub_2 (see Materials and Methods) and analyzed chemical shift perturbations upon titration with VHS. CSPs were also monitored on ^{15}N-VHS upon addition of K48-Ub_2 or K63-Ub_2. In the following discussion, the distal domain will be defined as the Ub unit which carries the free K48 or K63 side chain, whereas the proximal domain stands for the Ub unit that carries the free G76 residue. On VHS, both K63- and K48-Ub_2 target the same surface as monoUb (Figure 4a-d). Interestingly, unlike monoUb/VHS binding, several VHS residues experience strong signal attenuation for a [Ub_2]/[VHS] ratio as low as 0.1. Glu31, Trp33, Asp41, Asn82, Ala81, Lys111, and Val121 experience >50% decrease of their signal intensity when VHS binds K48-Ub_2. Likewise, the binding of VHS to K63-Ub_2 chains is accompanied by a >50% decrease in signal intensity for VHS residues Ala81, Asn82, Asp41, Glu31, and Trp33. Strong signal attenuation could reflect intermediate exchange between the free and ligand-bound states of the protein, due to slow on/off kinetics, but could also result from an increase in the apparent size of the molecule (slower tumbling). As a comparison, only VHS residues Trp33, Glu31, and Asp41 experienced a significant signal intensity decrease for the monoUb/VHS interaction.

On K63-Ub_2, VHS targets essentially the same surface either on the distal or in the proximal domain (Figure 4e−h) and shows similar CSP patterns. Perturbed residues cluster mainly around the Ub hydrophobic patch and are similar to the ones perturbed in monoUb. Moreover, either on the distal or in the proximal domain, K63-Ub_2 residues Gly47, Lys48, Gln49, Leu50, Val70, and Leu71 exhibit significant line broadening at a [VHS]/[Ub_2] ratio of 0.15. The same residues are also affected in monoUb upon binding to VHS. Additionally, the directions of the peak shifts observed for the hydrophobic residues in each Ub_2 subunits are identical to the one observed for the monoUb/VHS interaction. The latter findings suggest that the same mode of binding characterizes the interaction of VHS with K63-Ub2 and monoUb, consistent with the elongated structure of the K63-Ub_2 chains (*14*).

As evidenced in Figure 4i−l, the situation is somewhat different when dealing with the interaction of VHS with K48-Ub_2. Indeed, the distal domain exhibits higher CSPs than the proximal domain. The latter observation could be due to stronger binding but also to the opening−closing dynamics of the K48-Ub_2 chains (*67*). Although areas surrounding Leu8 and Val70 have similar peak shift magnitude for the K48-Ub_2 distal and proximal domains, peaks located close to Ile44 show weaker perturbations for the proximal domain (Figure 4k). This is most likely related to the fact that this region is bordered by the isopeptide bond linkage between the two Ub units. This linkage can play the role of a hinge and give rise to some steric hindrance, occluding the region surrounding Ile44. Most of the perturbed residues are located at the Ub/Ub interface in the closed conformation of the free Ub_2, suggesting a transition in the K48-Ub_2 conformation to allow the hydrophobic patch to become accessible. Moreover, the directions of the peak shifts affecting residues of the hydrophobic core (Leu8, Gln49, Leu50, Val70, Leu73) of the K48-Ub_2 proximal domain are significantly different from those experienced by the distal domain, the two subunits of K63-Ub_2 and monoUb. This suggests a different mode of binding for the proximal domain upon interaction with VHS. This assumption is also supported by the significant signal intensity decrease observed at a [VHS]/[Ub_2] ratio of 0.15. Indeed, Gly10, Ala46, Gly47, Val70, and Leu71 of the K48-Ub_2 distal domain experience a 50−80% signal intensity decrease whereas only residues located in the C-terminus of the K48-Ub_2 proximal domain are affected by a 30% signal intensity decrease, thus indicating a possible stronger binding of the distal domain to VHS.

VHS Binds Differently K48- and K63-Linked Ub_2. When observing the distal and proximal domains of both K48- and K63-Ub_2s, a striking contrast is apparent. In the case of K48-Ub_2, the CSP pattern exhibits a significant difference across the two domains in K48-Ub_2 (Figure 4i−l). The CSPs for the proximal domain of K48-Ub_2 exhibit much less perturbation than for the distal domain, indicating a stronger preference for

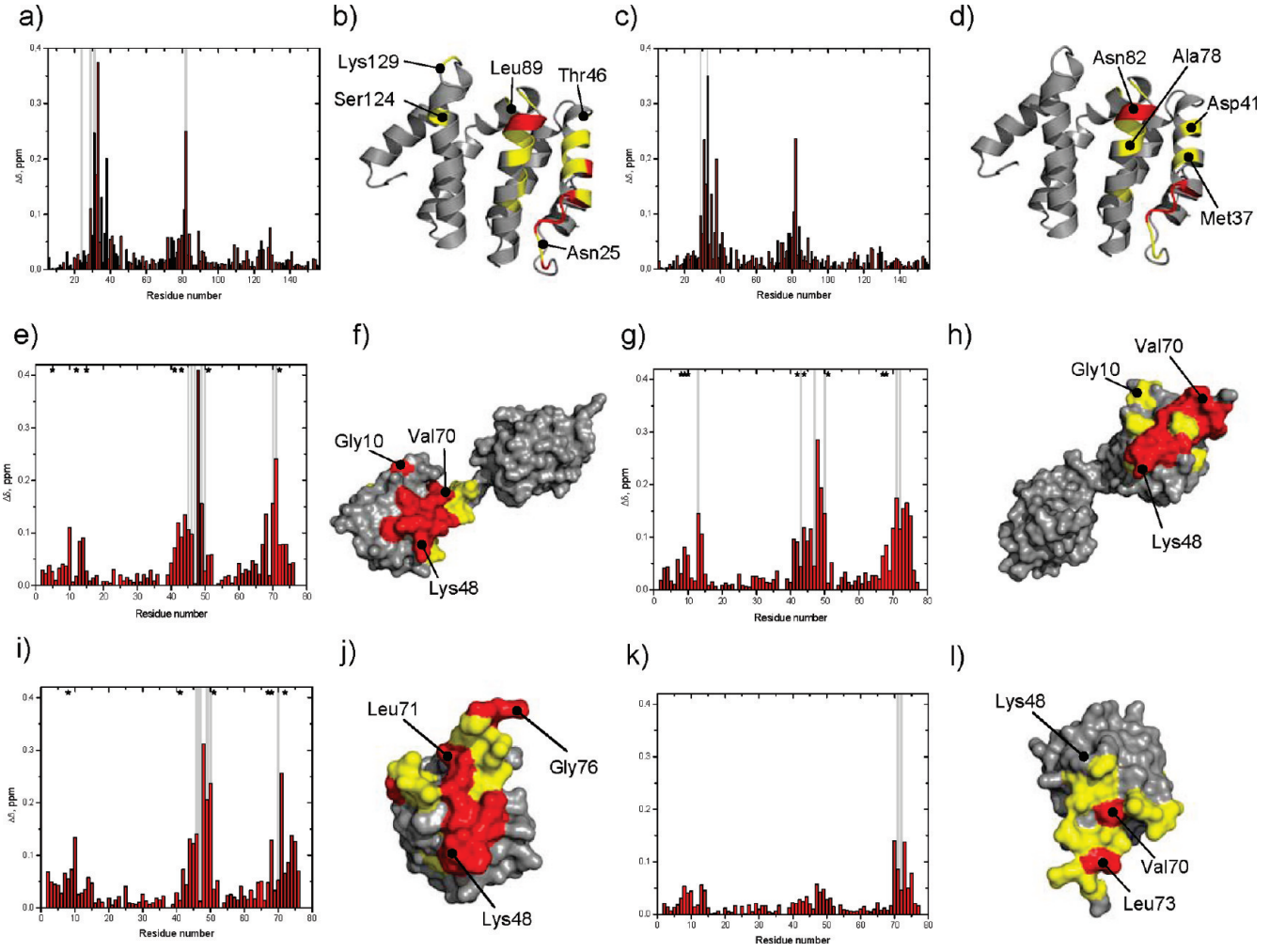

FIGURE 4: CSP mapping of the interaction of ^{15}N-VHS with K48-Ub_2 (a, b) and K63-Ub_2 (c, d) as well as the ^{15}N-K63-Ub_2 distal domain with VHS (e, f), the ^{15}N-K63-Ub_2 proximal domain with VHS (g, h), the ^{15}N-K48-Ub_2 distal domain with VHS (i, j), and the ^{15}N-K48-Ub_2 proximal domain with VHS (k, l). Residues experiencing intermediate exchange during the course of titration are represented by gray bars whereas residues affected by slow exchange are represented by black stars. Residues that exhibit significant shifts are colored red ($\Delta\delta > 0.1$) and yellow ($0.1 \geq \Delta\delta > 0.05$) except for the interaction of the ^{15}N-K48-Ub_2 proximal domain with VHS (l) where yellow residues indicate $0.1 \geq \Delta\delta > 0.04$. CSPs have been represented on the K48-Ub_2 (j, l) and K63-Ub_2 (f, h) structures (PDB codes 1AAR (*89*) and 2JF5 (*14*)).

VHS to bind to the distal domain. This conclusion is supported by several observations. First, more residues in the distal domain of K48-Ub_2 exhibit strong attenuations early in the titration with VHS, in contrast with the proximal domain (see gray bars in CSP plots in Figure 4i,k). Second, the K_d for residues in the distal domain is on average 5−6 times lower than for the proximal domain, suggesting tighter binding (compare 16 μM with 101 μM; see Table 1 and Supporting Information Figure SF12) whereas the derived K_d from the VHS side does not discriminate between the interaction with the distal and the proximal domain. Third, critical interacting residues around Lys48 in the proximal domain participate in the K48-G76 Ub_2 linkage which may occlude them from interacting with VHS. Conversely, these residues are available for interaction in the K63-linked Ub2. Fourth, under saturating conditions of the K48-Ub_2 distal domain, residues having a well-defined secondary structure yielded an average R_2 of 26.0 ± 1.8 s^{-1} with a standard deviation of 4.1 s^{-1} corresponding to a molecular mass range of 27.9−38.4 kDa with an average of 32 kDa. This result is consistent with an expected molecular mass of 34 kDa if one assumes a 1:1 stoichiometry. These important findings demonstrate that K48-Ub_2 can accommodate only one VHS molecule which can bind either one of the Ub_2 subunits with different binding affinities.

From the K63-Ub_2 side, the distal and the proximal domains each exhibit the same mode of binding for VHS. The latter assessment is supported by several observations. First, the CSP pattern at saturation is identical for both distal and proximal domains. Second, the same residues of the distal or the proximal domain of K63-Ub_2 (Gly47, Lys48, Gln49, Leu50, Val70) experience strong attenuation (>70%) early in the titration. Third, the K_d for residues in the distal domain is similar to the proximal domain (see Table 1 and Supporting Information Figure SF12). Fourth, K63-Ub_2 chains can accommodate up to two VHS molecules under saturating conditions as stated by our R_2 measurement on the K63-Ub_2 distal domain. The average R_2 is 35.7 ± 2.1 s^{-1} with a standard deviation of 6.2 s^{-1} giving rise to a molecular mass range of 42.4−58.1 kDa with an average of 45.4 kDa, consistent with both 2:1 stoichiometry and the known elongated structure of the K63-Ub2 chains (*14*).

A Possible Model for the Interaction of VHS with K48- and K63-Ub_2 Chains. According to our CSPs data for the VHS interaction with K48-Ub_2, it is clear that the VHS molecule did not experience any extended perturbation surface compared to the monoUb/VHS interaction. To better understand these results, we modeled the structure of both K48- and K63-Ub_2 chains in complex with VHS. We engineered T12C mutants for both the

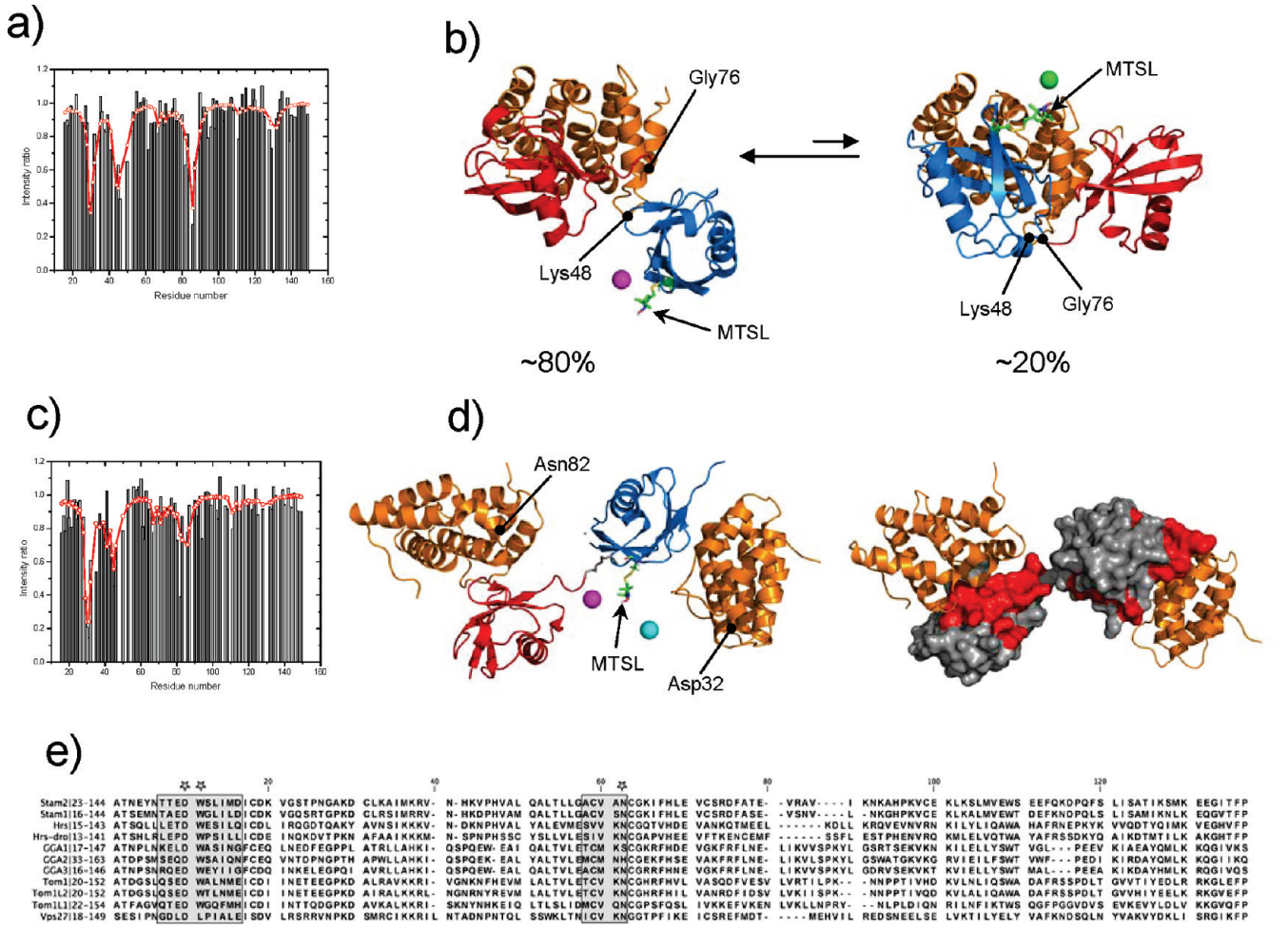

FIGURE 5: Analysis of the PRE data for VHS in the presence of a 1:1 equivalent of SL attached to the proximal domain of K48-Ub_2 at position C12 (a) and the proximal domain of K63-Ub_2 at position C12 (c). The reconstruction of the paramagnetic center yields two positions corresponding to two populations of the K48-Ub_2/VHS complex. Putative models of the K48-Ub_2/VHS complex are shown in (b). They show a relatively good agreement with the position of the paramagnetic centers (magenta and green sphere) and the theoretical position of MTSL for both populations. The distal and the proximal domains of K48-Ub_2 are represented in red and blue, respectively, whereas VHS is colored orange. Putative model of the K63-Ub_2/VHS complex (d) based on the monoUb/VHS complex. This model has been obtained by assuming that the paramagnetic spin label affects both VHS molecules under saturating conditions. The residues showing the largest chemical shift perturbations are represented by a red surface on the distal and the proximal domains of K63-Ub_2. (e) Sequence alignment of different VHS domains. The VHS surface affected upon binding to monoUb or Ub_2 is represented by gray squares whereas stars indicate the residues experiencing the highest CSPs.

K48- and K63-Ub_2 in their proximal domain (see Materials and Methods). We then recorded ^1H,^{15}N-HSQC spectra of VHS in the presence of SL attached to the proximal domain of K48-Ub_2 or K63-Ub_2 in oxidized and reduced conditions. As can be seen in Figure 5a for K48-Ub_2, the spin label affects regions on VHS which are different from the one seen for the interaction with C12-monoUb (Figure 3b). Indeed, it is noteworthy that three main areas are affected by at least a 60% decrease of signal intensity. These regions are characterized by residues Thr29, Thr30, Glu31, Ser45, Thr46, Ala50, Asn82, Ile86, Phe87, and Lys129, which are significantly affected by the spin label. Surprisingly, we were not able to reconstruct the position of the spin label by using one paramagnetic center only. Thus, we hypothesized that our PRE data could only originate from two populations (see Materials and Methods). The processing of our PRE data by means of two centers significantly improved the quality of the fit. Increasing the number of degrees of freedom is also supported by our *F* test calculation (see Supporting Information Figure SF13). Our results indicate two populated structures of 20% and 80% that correspond to two distinct positions of the paramagnetic center. For the highest populated structure, the distal domain interacts with the VHS domain in the same mode as for the monoUb/VHS interaction. The reconstruction of the two paramagnetic centers allowed us to model two different K48-Ub_2/VHS complexes by means of the Haddock software (*46*). As constraints, we used (i) CSPs obtained for VHS as well as the distal and the proximal domain of K48-Ub_2, (ii) unambiguous distances derived from MTSL attached to the proximal domain of K48-Ub_2 and a given proton of VHS, and (iii) unambiguous distances describing the isopeptide linkage between the distal and the proximal domain. A closer look at the modeled structure (Figure 5b) reveals the involvement of distal K48-Ub_2 residues Leu8, Val70, Ile44, Gly47, and Leu73 making contact with Trp33, Ala78, Ala81, and Asn82 of VHS, whereas the proximal residues Ile44, Val70, and Leu73 are in close proximity from Thr30 and Asn28 of VHS. The latter findings are consistent with our CSPs and titration data indicating that the VHS domain can bind the distal or the proximal domain. For comparison, we recorded a HSQC spectrum of ^{15}N-labeled VHS in the presence of K63-Ub_2 harboring a MTSL spin label at position C12 on its proximal domain. As can be seen in Figure 5c, the picture is different from K48-Ub_2 as residues located around Glu31 experience

a stronger decrease in signal intensity. Surprisingly, regions surrounding Ser45 and Asn82 are also slightly affected. It is important to remember that our CSPs and spin relaxation data indicate that K63-Ub_2 can accommodate two VHS molecules under saturating conditions. As a consequence, our data suggest that the spin label could affect not only the VHS molecule bound to the proximal domain but also the VHS molecule bound to the distal domain if sufficiently close. This led us to consider two possible positions of the spin label. To check our hypothesis, we aligned the previously determined monoUb/VHS structure with the crystal structure of K63-Ub_2 (*14*). As can be seen in Figure 5d, our putative model can account for the position of the attached spin label. The latter one would affect VHS bound to the distal or the proximal domain of K63-Ub2 at the same time. This gives rise to a K63-Ub_2 structure where the proximal domain is somewhat rotated around the G76-K63 isopeptide bond which is, in fact, not surprising if one considers a certain flexibility of this bond as previously reported (*15*).

DISCUSSION

According to our CSP data analysis, VHS binds monoUb with an average K_d of 60 ± 7 μM (Table 1) where electrostatic interactions play a role. The kinetics of binding between monoUb and VHS is characterized by k_{on} and k_{off} values of $(\sim 1.3 \pm 0.1) \times 10^8$ M^{-1} s^{-1} and 7040 ± 350 s^{-1}, respectively. This fast dissociation rate has important implications and suggests that the VHS domain interactions are optimized for the rapid assembly and disassembly of protein complexes, consistent with cargo sorting. The K_d value is consistent with affinities usually reported for different UBD/monoUb complexes (*26*, *27*) (in the micromolar range).

The affinity of various VHS domains for monoUb varies in a range 190−2100 μM (*68*). Additionally, the Stam2-VHS domain shows slightly stronger affinity for polyUb chains and more particularly for the distal domain of K63-Ub_2. Thus, suitable questions are (1) "Why do different VHS domains exhibit different binding affinities for monoUb?" and (2) "Is there a unique structural feature that allows a tighter binding between VHS and K63-linked polyUb chains?"

How Different Are VHS Domains? The VHS domain is present in eight mammalian proteins (GGA1/2/3, Hrs, Stam1:2, Tom1, and Srcasm) where it occupies the N-terminal end suggesting that its positioning is important for its function (*30*, *69*). The VHS domain of Stam2 interacts with monoUb via its concave surface and primarily involves residues located on helices α2 and α4. We find that the VHS domain recognizes a region on monoUb centered on Ile13, Lys48, and Val70 which is essential for its function as a sorting signal (*70*−*73*). The latter surface is in sharp contrast with the one observed on monoUb in previous studies in solution (*74*). The observed differences could be due to the fact that the Ub/Stam2 interaction was carried out in the cell in the presence of full-length Stam2. Moreover, it is noteworthy that the relative orientation of monoUb with respect to VHS (Figure 3c) allows Lys63 to be freely available for Lys63 polyubiquitin chain formation whereas Lys48 is sequestered at the interface between VHS and monoUb. This observation might have further implication in the binding mode of Lys63-diubiquitin chains to VHS, as Lys63-polyubiquitin chains have been shown to facilitate endocytosis (*11*, *22*, *75*).

Among the eight mammalian proteins containing a VHS domain, the VHS domain of the Stam family has been reported to bind monoUb with the lowest K_d (*30*, *32*, *33*), and the deletion of the VHS domain from the full-length Stam1 or 2 dramatically reduced their ubiquitin binding (*30*), thus indicating that the VHS domain of Stam proteins is of prime importance.

The Stam1 protein is a Stam2 isoform (*76*) and shares 74% identity with Stam2 (Figure 5e). If one considers the orientation of Ub with respect to VHS, our monoUb/VHS structure is slightly different from the recently published Ub/Stam1-VHS structure (PDB code 3LDZ) (*68*). Indeed, monoUb is translated 3.5 Å toward the VHS α2 helix whereas the monoUb α-helix is rotated approximately 20° with respect to monoUb in the monoUb/Stam1-VHS crystal structure. Moreover, our structure is in sharp contrast with a predicted model using the Dsk2 UBA domain (*33*) in a sense that the α2 helix of the VHS domain is tilted by 50° from the predicted model. The interaction surfaces on Stam1 and Stam2 are similar and mainly involve conserved residues except Stam2 Ser34 and Ala81 which are replaced in Stam1 by Gly27 and Ser74, respectively. Thus, the residues conserved only in Stam proteins are likely to play an important role in ubiquitin binding because the sequence homology of the VHS domains between Stam1 and 2 is much higher than that between Stam proteins and others (<37%).

Stam2 is tightly associated with Hrs to form the ESCRT-0 complex which sorts ubiquitinated transmembrane proteins for lysosomal degradation through the ESCRT machinery (*23*, *29*, *77*−*81*). Furthermore, Hrs binds Ub by its DUIM (double-sided ubiquitin interacting motif) with a K_d in the range of 200−400 μM (*32*, *82*, *83*) whereas the VHS domain of Hrs yields a 23 times higher K_d than the VHS of Stam2 (*68*). Interestingly, the FYVE domain, which is located in-between the VHS and UIM domains, is interacting with VHS in an intra- and intermolecular manner (*84*). The interaction between the VHS and FYVE domains of Hrs mainly occurs through residues located on the VHS α2 helix. Hrs residues Trp23 and Asp31 which are conserved in Stam2 (counterpart Trp33 and Asp41) are engaged in hydrophobic and hydrogen-bonding interactions, respectively. Other interacting residues of Hrs Pro21, Pro24, and Leu27 which are not conserved in Stam2 (counterpart Glu31, Ser34, and Met37) are involved in hydrophobic contacts with FYVE. Thus, the counterpart residues of Hrs which are involved in the interaction of the Stam2 VHS domain with monoUb are sequestered at the interface between VHS and FYVE. As a consequence, the FYVE domain might compete with monoUb and is likely to decrease the binding affinity of VHS for monoUb. As can be seen, Ub binding is a general property of most of the VHS domains where highly conserved residues Asp32, Trp33, and Asn82 are likely to play an important role. The replacement of these residues or surrounding residues by residues harboring different electrostatic charges is prone to lower the interaction with Ub.

Insights into the VHS Preferences for Polyubiquitin Chains. The question of "How does the VHS domain bind polyubiquitin and more particularly K48- and K63-linked Ub_2" remains open. The question is of prime importance as K63 polyubiquitination appears to be the major signal for cargo sorting into the MVB pathway (*20*). Our results show a slightly higher affinity for Ub_2 chains than for monoUb with linkage-dependent modes of binding with respect to VHS. Specifically, we report here asymmetric binding of K48-Ub_2 to VHS where the proximal domain exhibits a 5-fold weaker dissociation constant than the distal domain. Moreover, we found two different populated structures in solution, likely reflecting the complexity of this binding event. Such a situation has been reported earlier for other UBDs (*85*). The apparent dissociation constant measured on the

VHS side is 43 μM, which is a 1.5 times increase with respect to the binding affinity for monoUb (Table 1). This noticeable difference between the two Ub_2 chains with respect to their VHS binding sheds light on the possible consequences in cargo sorting and a possible explanation of the preference for K63- over K48-Ub_2 chains.

The lower K_d (hence tighter binding) seen from the distal K48-Ub_2 side may have different explanations if one looks at the most populated structure (Figure 5b): First, as seen from CSPs, Gly76 exhibits a much stronger perturbation compared to monoUb. It is then likely that this residue offers another anchoring point for VHS by extending the binding interface toward the proximal domain. The analysis of the interface reveals that the side chains of the distal residues Arg74 and Gly76 could interact with Asp41 and Ser 34 of VHS. It is noteworthy that these interactions were not present in the structure of the monoUb/VHS complex. At the same time, Gly47, Gln49, and Arg74 of the proximal domain are in close contact with Asp32 and Tyr 27 of VHS. Second, the interaction of the K48-Ub_2 chain gives rise to an extended burried surface area of 1803 Å^2 compared to 1138 Å^2 for the monoUb/VHS complex, thus rendering the formation of the complex in this case entropically favorable.

To understand the difference in binding affinity observed for each of the K48-Ub_2 subunits, we investigated chemical shift perturbations at an early stage in the titration ([VHS]/[Ub_2] = 0.1). Here, Phe45, Gly47, Leu50, Val70, and Leu71 are the first perturbed residues on the distal domain and also experience intermediate exchange with a decrease of their signal intensity of 70%, indicating possible strong interaction with VHS. In contrast, Thr9, Arg42, Val70, Leu71, and Leu73 are the first perturbed residues on the proximal domain and are located in an opposite region from the one constituted by the Gly76−Lys48 isopeptide bond. On the proximal domain, Val70, Leu71, and Leu73 experience a decrease of their signal intensity by 60% early in the titration. Moreover, the magnitude and the directions of the shifts in the signals are different with those associated with the opening and closing of K48-Ub_2. Thus, it is unlikely that the weak perturbations seen for the proximal domain are due to the loss of hydrophobic contactes between the two Ub moieties. As previous studies have shown that the Ub/Ub interface of K48-Ub_2 is dynamic in solution (*5*), we can consider a possible mechanistic event where VHS binds first the partially open Ub_2 interdomain interface. As the interface opens further upon titration with VHS, the distal residues Arg72 to Gly76 become strongly perturbed. To date, this is the first experimental evidence that the VHS domain of Stam2 enters the hydrophobic pocket of K48-Ub_2 to bind directly to each Ub subunit with a different affinity.

The observed weaker binding of the proximal domain to VHS may be explained by the fact that Lys48, which is the most affected residue in the monoUb/VHS interaction (Figure 1d), participates in the Gly76−Lys48 isopeptide bond. As a consequence, the Lys48 residue of the proximal domain may be less able to interact with VHS and may have a negative effect on the Ub_2/VHS binding. Conversely, the Gly76 residue of the distal domain is significantly perturbed compared to its interaction with monoUb. A possible explanation is a higher accessibility of Gly76 owing to the opening of the hydrophobic interface, allowing the Gly76 residue to directly interact with VHS. Our observations are unique with respect to what has been previously reported with other protein interactions involving diverse UBDs and K48-Ub_2 chains. For instance, the proximal Ub appears to be the primary binding site for hHR23A-UBA which binds to Ub_2 in a sandwich-like fashion whereas the UQ1-UBA does not show any preference for either of the two Ub_2 subunits. Diverse modes of binding to K48-Ub_2 may arise from a compromise between the size of the receptor which could give rise to steric constraints (hence preventing K48-Ub_2 to wrap around the ligand) and the electrostatic surface of the receptor which could offer a second binding site to another Ub_2 subunit. Binding between VHS and K48-linked chains could be complicated by the fact that the functionally important hydrophobic residues are sequestered at the interface at neutral pH. K48-Ub_2 chains are predominantly closed at neutral pH whereas binding to the VHS domain requires the open conformation of the K48-Ub2 chain. Indeed, the opening of the hydrophobic interface is essential for polyubiquitin's binding, and locking the interface would preclude any VHS (or other lingands) binding (*86*). As a consequence, the VHS domain, or possibly other UBD components of the Stam2/Hrs complex, must find the proper open candidate prior to binding. The sequestered nature of the Ub/Ub interface would then slow down the entry into the MVB pathway. Considering that the VHS domain is present in many proteins involved in the endocytic pathway, our results provide a possible explanation for the increased efficiency of multimonoubiquitination or K63-linked polyubiquitination signals over K48-linked chains for cargo delivery to the lysosome (*22*, *87*).

K63-Ub_2 adopts a different mode of binding to VHS that is more similar to monoUb/VHS binding. Each of the K63-Ub_2 subunits can accommodate one VHS molecule under saturating conditions. Indeed, VHS binds K63-Ub_2 chains with no preference for the distal or the proximal domain and exhibits a dissociation constant in the range 30−40 μM (Table 1). It has to be recalled here that K63-Ub_2 adopts an elongated structural conformation. Consequently, the hydrophobic patch of K63-Ub_2 presents a higher accessibility to VHS and can bind as two independent Ub sites with no cooperativity as exhibited by the titration curves (Supporting Information Figure SF12).

According to our results, it is likely that the VHS domain recognizes a given topology/structure of polyUb chains which favors its interaction with the Ub hydrophobic patch. The extended conformation of K63-Ub_2 exposes the Ub hydrophobic patch on both subunits and offers the possibility for direct interactions with VHS without the need to compete with an opening/closing equilibrium of the Ub/Ub interface. We can speculate that K63-linked chains harbor a better accessibility of Ub subunits and can then accommodate more than one UBD per chains owing to avid binding (*88*). Our predicted model for the interaction of VHS with K63-Ub_2 along with the 2:1 stoichiometry of this complex has further implication in the binding of Stam2 to polyubiquitin and cargo sorting. In the context of the whole Stam2 protein which contains the VHS and UIM domains connected by a 20 amino acid linker, we can reasonably predict a possible structural organization involving VHS-UIM and K63-Ub_2. According to the orientation of the VHS domain with respect to monoUb as well as K63-Ub_2, it is likely that the VHS domain might bind one Ub moiety whereas the UIM domain might bind the other Ub subunit of K63-Ub_2, leading to an increase of the affinity of the interaction. Nevertheless, we cannot exclude other lowly populated structures giving rise to another organization. Conversely, it seems unlikely that K48-Ub_2 chains can accommodate more than one UBD (besides VHS), because of steric hindrance and the 1:1 stoichiometry of the VHS/K48-Ub_2 equilibrium. Recognition of the K48-Ub_2 chains by the VHS-UIM domains might be complicated by several factors.

First, according to the stoichiometry of the VHS/K48-Ub2 complex, we can reasonably predict that two K48-Ub_2 will be necessary to bind the VHS-UIM domains. Second, according to the fact that an average of 15% of K48-Ub_2 chains are in an open conformation at neutral pH (*5*), it is likely that the recognition of K48-linked chains by the VHS-UIM domains will not be kinetically favorable. The combination of these factors could give rise to a less efficient sorting of K48- compared to K63-polyubiquitinated targets. These hypotheses, of course, have to be confirmed by further structural studies which should provide insight into the advantages (if any) that might be offered by such structural organization.

ACKNOWLEDGMENT

The authors thank David Fushman for insightful discussions and for hosting A.L. for the Ub2 chain synthesis. We thank Carlos Castañeda for careful reading of the manuscript and useful comments. We also acknowledge the French Rhone Alpes region for the ExploraDoc fellowship which allowed the expression of the Ub_2 chains. We thank the Rikken Institute for providing us the NMR assignments corresponding to the Stam2-VHS structure previously released under PDB code 1X5B. The eNMR project, supported by the National GRID Initiatives of Italy, Germany, and the Dutch BiG Grid project (Netherlands Organization for Scientific Research) is acknowledged for the use of web portals, computing, and storage facilities.

SUPPORTING INFORMATION AVAILABLE

Two tables, ST1 and ST2, and 13 figures, SF1−SF13, showing different spectra, relaxation data, and PRE data analysis. This material is available free of charge via the Internet at http://pubs.acs.org.

REFERENCES

1. Hicke, L., and Dunn, R. (2003) Regulation of membrane protein transport by ubiquitin and ubiquitin-binding proteins. *Annu. Rev. Cell Dev. Biol. 19*, 141–172.
2. Haglund, K., Di Fiore, P. P., and Dikic, I. (2003) Distinct monoubiquitin signals in receptor endocytosis. *Trends Biochem. Sci. 28*, 598–603.
3. Pickart, C. M., and Fushman, D. (2004) Polyubiquitin chains: polymeric protein signals. *Curr. Opin. Chem. Biol. 8*, 610–616.
4. Cook, W. J., Jeffrey, L. C., Kasperek, E., and Pickart, C. M. (1994) Structure of tetraubiquitin shows how multiubiquitin chains can be formed. *J. Mol. Biol. 236*, 601–609.
5. Varadan, R., Walker, O., Pickart, C. M., and Fushman, D. (2002) Structural properties of polyubiquitin chains in solution. *J. Mol. Biol. 324*, 637–647.
6. Dijk, A., Fushman, D., and Bonvin, A. (2005) Various strategies of using residual dipolar couplings in NMR-driven protein docking: application to Lys48-linked di-ubiquitin and validation against ^{15}N-relaxation data. *Proteins 60*, 367–381.
7. Eddins, M. J., Varadan, R., Fushman, D., Pickart, C. M., and Wolberger, C. (2007) Crystal structure and solution NMR studies of Lys48-linked tetraubiquitin at neutral pH. *J. Mol. Biol. 367*, 204–211.
8. Spence, J., Sadis, S., Haas, A., and Finley, D. (1995) A ubiquitin mutant with specific defects in DNA repair and multiubiquitination. *Mol. Cell. Biol. 15*, 1265.
9. Hicke, L. (1999) Gettin' down with ubiquitin: turning off cell-surface receptors, transporters and channels. *Trends Cell Biol. 9*, 107–112.
10. Sun, L., and Chen, Z. J. (2004) The novel functions of ubiquitination in signaling. *Curr. Opin. Cell. Biol. 16*, 119–126.
11. Mukhopadhyay, D., and Riezman, H. (2007) Proteasome-independent functions of ubiquitin in endocytosis and signaling. *Science 315*, 201–205.
12. Tenno, T., Fujiwara, K., Tochio, H., Iwai, K., Morita, E. H., Hayashi, H., Murata, S., Hiroaki, H., Sato, M., Tanaka, K., and Shirakawa, M. (2004) Structural basis for distinct roles of Lys63- and Lys48-linked polyubiquitin chains. *Genes Cells 9*, 865–875.
13. Varadan, R., Assfalg, M., Haririnia, A., Raasi, S., Pickart, C. M., and Fushman, D. (2004) Solution conformation of Lys63-linked di-ubiquitin chain provides clues to functional diversity of polyubiquitin signaling. *J. Biol. Chem. 279*, 7055–7063.
14. Komander, D., Reyes-Turcu, F., Licchesi, J. D., Odenwaelder, P., Wilkinson, K. D., and Barford, D. (2009) Molecular discrimination of structurally equivalent Lys 63-linked and linear polyubiquitin chains, *EMBO Rep.* (in press).
15. Datta, A. B., Hura, G. L., and Wolberger, C. (2009) The structure and conformation of Lys63-linked tetraubiquitin. *J. Mol. Biol. 392*, 1117–1124.
16. Hicke, L. (2001) Protein regulation by monoubiquitin. *Nat. Rev. Mol. Cell Biol. 2*, 195–201.
17. Mosesson, Y., Shtiegman, K., Katz, M., Zwang, Y., Vereb, G., Szollosi, J., and Yarden, Y. (2003) Endocytosis of receptor tyrosine kinases is driven by monoubiquitylation, not polyubiquitylation. *J. Biol. Chem. 278*, 21323–21326.
18. Duncan, L. M., Piper, S., Dodd, R. B., Saville, M. K., Sanderson, C. M., Luzio, J. P., and Lehner, P. J. (2006) Lysine-63-linked ubiquitination is required for endolysosomal degradation of class I molecules. *EMBO J. 25*, 1635–1645.
19. Huang, T. T., and D'Andrea, A. D. (2006) Regulation of DNA repair by ubiquitylation. *Nat. Rev. Mol. Cell. Biol. 7*, 323–334.
20. Lauwers, E., Jacob, C., and Andre, B. (2009) K63-linked ubiquitin chains as a specific signal for protein sorting into the multivesicular body pathway. *J. Cell Biol. 185*, 493–502.
21. Stawiecka-Mirota, M., Pokrzywa, W., Morvan, J., Zoladek, T., Haguenauer-Tsapis, R., Urban-Grimal, D., and Morsomme, P. (2007) Targeting of Sna3p to the endosomal pathway depends on its interaction with Rsp5p and multivesicular body sorting on its ubiquitylation. *Traffic 8*, 1280–1296.
22. Barriere, H., Nemes, C., Du, K., and Lukacs, G. L. (2007) Plasticity of polyubiquitin recognition as lysosomal targeting signals by the endosomal sorting machinery. *Mol. Biol. Cell 18*, 3952–3965.
23. Hurley, J. H., and Emr, S. D. (2006) The ESCRT complexes: structure and mechanism of a membrane-trafficking network. *Annu. Rev. Biophys. Biomol. Struct. 35*, 277–298.
24. Hurley, J. H. (2008) ESCRT complexes and the biogenesis of multivesicular bodies. *Curr. Opin. Cell. Biol. 20*, 4–11.
25. Hurley, J. H., and Ren, X. (2009) The circuitry of cargo flux in the ESCRT pathway. *J. Cell Biol. 185*, 185–187.
26. Hicke, L., Schubert, H. L., and Hill, C. P. (2005) Ubiquitin-binding domains. *Nat. Rev. Mol. Cell. Biol. 6*, 610–621.
27. Hurley, J. H., Lee, S., and Prag, G. (2006) Ubiquitin-binding domains. *Biochem. J. 399*, 361–372.
28. Dikic, I., Wakatsuki, S., and Walters, K. J. (2009) Ubiquitin-binding domains—from structures to functions. *Nat. Rev. Mol. Cell. Biol. 10*, 659–671.
29. Shields, S. B., Oestreich, A. J., Winistorfer, S., Nguyen, D., Payne, J. A., Katzmann, D. J., and Piper, R. (2009) ESCRT ubiquitin-binding domains function cooperatively during MVB cargo sorting. *J. Cell Biol. 185*, 213–224.
30. Mizuno, E., Kawahata, K., Kato, M., Kitamura, N., and Komada, M. (2003) STAM proteins bind ubiquitinated proteins on the early endosome via the VHS domain and ubiquitin-interacting motif. *Mol. Biol. Cell 14*, 3675–3689.
31. Mizuno, E., Kawahata, K., Okamoto, A., Kitamura, N., and Komada, M. (2004) Association with Hrs is required for the early endosomal localization, stability, and function of STAM. *J. Biochem. 135*, 385–396.
32. Ren, X., Kloer, D. P., Kim, Y. C., Ghirlando, R., Saidi, L. F., Hummer, G., and Hurley, J. H. (2009) Hybrid structural model of the complete human ESCRT-0 complex. *Structure 17*, 406–416.
33. Hong, Y. H., Ahn, H. C., Lim, J., Kim, H. M., Ji, H. Y., Lee, S., Kim, J. H., Park, E. Y., Song, H. K., and Lee, B. J. (2009) Identification of a novel ubiquitin binding site of STAM1 VHS domain by NMR spectroscopy. *FEBS Lett. 583*, 287–292.
34. Delaglio, F., Grzesiek, S., Vuister, G. W., Zhu, G., Pfeifer, J., and Bax, A. (1995) NMRPipe: a multidimensional spectral processing system based on UNIX pipes. *J. Biomol. NMR 6*, 277–293.
35. Goddard, T. D., Kneller, D. G. SPARKY 3, University of California, San Francisco, CA.
36. Cornilescu, G., Delaglio, F., and Bax, A. (1999) Protein backbone angle restraints from searching a database for chemical shift and sequence homology. *J. Biomol. NMR 13*, 289–302.

37. Shen, Y., Lange, O., Delaglio, F., Rossi, P., Aramini, J. M., Liu, G., Eletsky, A., Wu, Y., Singarapu, K. K., Lemak, A., Ignatchenko, A., Arrowsmith, C. H., Szyperski, T., Montelione, G. T., Baker, D., and Bax, A. (2008) Consistent blind protein structure generation from NMR chemical shift data. *Proc. Natl. Acad. Sci. U.S.A. 105*, 4685–4690.
38. Shen, Y., Vernon, R., Baker, D., and Bax, A. (2009) De novo protein structure generation from incomplete chemical shift assignments. *J. Biomol. NMR 43*, 63–78.
39. Fushman, D., Cahill, S., and Cowburn, D. (1997) The main-chain dynamics of the dynamin pleckstrin homology (PH) domain in solution: analysis of ^{15}N relaxation with monomer/dimer equilibration. *J. Mol. Biol. 266*, 173–194.
40. Kay, L. E., Torchia, D. A., and Bax, A. (1989) Backbone dynamics of proteins as studied by ^{15}N inverse detected heteronuclear NMR spectroscopy: application to staphylococcal nuclease. *Biochemistry 28*, 8972–8979.
41. Johnson, B. A., and Blevins, R. A. (1994) NMR View: a computer program for the visualization and analysis of NMR data. *J. Biomol. NMR 4*, 603–614.
42. Walker, O., Varadan, R., and Fushman, D. (2004) Efficient and accurate determination of the overall rotational diffusion tensor of a molecule from (15)N relaxation data using computer program ROTDIF. *J. Magn. Reson. 168*, 336–345.
43. Cantor, C. R., and Schimmel, P. R. (1980) Biophysical Chemistry, Part II, W. H. Freeman, New York.
44. Kovrigin, E. L., and Loria, J. P. (2006) Enzyme dynamics along the reaction coordinate: critical role of a conserved residue. *Biochemistry 45*, 2636–2647.
45. Dominguez, C., Boelens, R., and Bonvin, A. (2003) HADDOCK: a protein-protein docking approach based on biochemical or biophysical information. *J. Am. Chem. Soc. 125*, 1731–1737.
46. Vries, S., Dijk, A., Krzeminski, M., Dijk, M., Thureau, A., Hsu, V., Wassenaar, T., and Bonvin, A. M. (2007) HADDOCK versus HADDOCK: new features and performance of HADDOCK2.0 on the CAPRI targets. *Proteins 69*, 726–733.
47. Varadan, R., Assfalg, M., and Fushman, D. (2005) Using NMR spectroscopy to monitor ubiquitin chain conformation and interactions with ubiquitin-binding domains. *Methods Enzymol. 399*, 177–192.
48. Jain, N. U., Venot, A., Umemoto, K., Leffler, H., and Prestegard, J. H. (2001) Distance mapping of protein-binding sites using spin-labeled oligosaccharide ligands. *Protein Sci. 10*, 2393–2400.
49. Battiste, J. L., and Wagner, G. (2000) Utilization of site-directed spin labeling and high-resolution heteronuclear nuclear magnetic resonance for global fold determination of large proteins with limited nuclear overhauser effect data. *Biochemistry 39*, 5355–5365.
50. Fushman, D., Varadan, R., Assfalg, M., and Walker, O. (2004) Determining domain orientation in macromolecules by using spin-relaxation and residual dipolar coupling measurements. *Prog. Magn. Reson. Spectrosc. 44*, 189–214.
51. Ryabov, Y., and Fushman, D. (2006) Interdomain mobility in di-ubiquitin revealed by NMR. *Proteins 63*, 787–796.
52. Zuiderweg, E. R. (2002) Mapping protein-protein interactions in solution by NMR spectroscopy. *Biochemistry 41*, 1–7.
53. Vaynberg, J., and Qin, J. (2006) Weak protein-protein interactions as probed by NMR spectroscopy. *Trends Biotechnol. 24*, 22–27.
54. O'Connell, M. R., Gamsjaeger, R., and Mackay, J. P. (2009) The structural analysis of protein-protein interactions by NMR spectroscopy. *Proteomics 9*, 5224–5232.
55. Dijk, A., Kaptein, R., Boelens, R., and Bonvin, A. (2006) Combining NMR relaxation with chemical shift perturbation data to drive protein-protein docking. *J. Biomol. NMR 34*, 237–244.
56. Bruschweiler, R., Liao, X., and Wright, P. E. (1995) Long-range motional restrictions in a multidomain zinc-finger protein from anisotropic tumbling. *Science 268*, 886–889.
57. Tjandra, N., Garrett, D. S., Gronenborn, A. M., Bax, A., and Clore, G. M. (1997) Defining long range order in NMR structure determination from the dependence of heteronuclear relaxation times on rotational diffusion anisotropy. *Nat. Struct. Biol. 4*, 443–449.
58. Ryabov, Y., and Fushman, D. (2007) Structural assembly of multidomain proteins and protein complexes guided by the overall rotational diffusion tensor. *J. Am. Chem. Soc. 129*, 7894–7902.
59. Fushman, D., Xu, R., and Cowburn, D. (1999) Direct determination of changes of interdomain orientation on ligation: use of the orientational dependence of ^{15}N NMR relaxation in Abl SH(32). *Biochemistry 38*, 10225–10230.
60. Ghose, R., Fushman, D., and Cowburn, D. (2001) Determination of the rotational diffusion tensor of macromolecules in solution from NMR relaxation data with a combination of exact and approximate methods—application to the determination of interdomain orientation in multidomain proteins. *J. Magn. Reson. 149*, 204–217.
61. Clore, G. M., and Iwahara, J. (2009) Theory, practice, and applications of paramagnetic relaxation enhancement for the characterization of transient low-population states of biological macromolecules and their complexes. *Chem. Rev. 109*, 4108–4139.
62. Su, X. C., and Otting, G. (2010) Paramagnetic labelling of proteins and oligonucleotides for NMR. *J. Biomol. NMR 46*, 101–112.
63. Otting, G. (2010) Protein NMR using paramagnetic ions. *Annu. Rev. Biophys. 39*, 387–405.
64. Berliner, L. J., Grunwald, J., Hankovszky, H. O., and Hideg, K. (1982) A novel reversible thiol-specific spin label: papain active site labeling and inhibition. *Anal. Biochem. 119*, 450–455.
65. Brunger, A. T., Adams, P. D., Clore, G. M., DeLano, W. L., Gros, P., Grosse-Kunstleve, R. W., Jiang, J. S., Kuszewski, J., Nilges, M., Pannu, N. S., Read, R. J., Rice, L. M., Simonson, T., and Warren, G. L. (1998) Crystallography & NMR system: a new software suite for macromolecular structure determination. *Acta Crystallogr., Sect. D: Biol. Crystallogr. 54*, 905–921.
66. Cornilescu, G., Marquardt, J. L., Ottiger, M., and Bax, A. (1998) Validation of protein structure from anisotropic carbonyl chemical shifts in a dilute liquid crystalline phase. *J. Am. Chem. Soc. 120*, 6836–6837.
67. Sims, J. J., Haririnia, A., Dickinson, B. C., Fushman, D., and Cohen, R. E. (2009) Avid interactions underlie the Lys63-linked polyubiquitin binding specificities observed for UBA domains. *Nat. Struct. Mol. Biol. 16*, 883–889.
68. Ren, X., and Hurley, J. H. (2010) VHS domains of ESCRT-0 cooperate in high-avidity binding to polyubiquitinated cargo. *EMBO J. 29*, 1045–1054.
69. Lohi, O., Poussu, A., Mao, Y., Quiocho, F., and Lehto, V. P. (2002) VHS domain—a longshoreman of vesicle lines. *FEBS Lett. 513*, 19–23.
70. Nakatsu, F., Sakuma, M., Matsuo, Y., Arase, H., Yamasaki, S., Nakamura, N., Saito, T., and Ohno, H. (2000) A di-leucine signal in the ubiquitin moiety. Possible involvement in ubiquitination-mediated endocytosis. *J. Biol. Chem. 275*, 26213–26219.
71. Shih, S. C., Sloper-Mould, K. E., and Hicke, L. (2000) Monoubiquitin carries a novel internalization signal that is appended to activated receptors. *EMBO J. 19*, 187–198.
72. Sloper-Mould, K. E., Jemc, J. C., Pickart, C. M., and Hicke, L. (2001) Distinct functional surface regions on ubiquitin. *J. Biol. Chem. 276*, 30483–30489.
73. Shih, S. C., Katzmann, D. J., Schnell, J. D., Sutanto, M., Emr, S. D., and Hicke, L. (2002) Epsins and Vps27p/Hrs contain ubiquitin-binding domains that function in receptor endocytosis. *Nat. Cell Biol. 4*, 389–393.
74. Burz, D. S., Dutta, K., Cowburn, D., and Shekhtman, A. (2006) Mapping structural interactions using in-cell NMR spectroscopy (STINT-NMR). *Nat. Methods 3*, 91–93.
75. Galan, J. M., and Haguenauer-Tsapis, R. (1997) Ubiquitin lys63 is involved in ubiquitination of a yeast plasma membrane protein. *EMBO J. 16*, 5847–5854.
76. Endo, K., Takeshita, T., Kasai, H., Sasaki, Y., Tanaka, N., Asao, H., Kikuchi, K., Yamada, M., Chenb, M., O'Shea, J. J., and Sugamura, K. (2000) STAM2, a new member of the STAM family, binding to the Janus kinases. *FEBS Lett. 477*, 55–61.
77. Asao, H., Sasaki, Y., Arita, T., Tanaka, N., Endo, K., Kasai, H., Takeshita, T., Endo, Y., Fujita, T., and Sugamura, K. (1997) Hrs is associated with STAM, a signal-transducing adaptor molecule. Its suppressive effect on cytokine-induced cell growth. *J. Biol. Chem. 272*, 32785–32791.
78. Bach, I., and Ostendorff, H. P. (2003) Orchestrating nuclear functions: ubiquitin sets the rhythm. *Trends Biochem. Sci. 28*, 189–195.
79. Babst, M. (2005) A protein's final ESCRT. *Traffic 6*, 2–9.
80. Bowers, K., and Stevens, T. H. (2005) Protein transport from the late Golgi to the vacuole in the yeast *Saccharomyces cerevisiae*. *Biochim. Biophys. Acta 1744*, 438–454.
81. Slagsvold, T., Pattni, K., Malerod, L., and Stenmark, H. (2006) Endosomal and non-endosomal functions of ESCRT proteins. *Trends Cell Biol. 16*, 317–326.
82. Raiborg, C., Bache, K. G., Gillooly, D. J., Madshus, I. H., Stang, E., and Stenmark, H. (2002) Hrs sorts ubiquitinated proteins into clathrin-coated microdomains of early endosomes. *Nat. Cell Biol. 4*, 394–398.
83. Hirano, S., Kawasaki, M., Ura, H., Kato, R., Raiborg, C., Stenmark, H., and Wakatsuki, S. (2006) Double-sided ubiquitin binding of Hrs-UIM in endosomal protein sorting. *Nat. Struct. Mol. Biol. 13*, 272–277.
84. Mao, Y., Nickitenko, A., Duan, X., Lloyd, T. E., Wu, M. N., Bellen, H., and Quiocho, F. A. (2000) Crystal structure of the VHS and

FYVE tandem domains of Hrs, a protein involved in membrane trafficking and signal transduction. *Cell 100*, 447–456.
85. Zhang, N., Wang, Q., Ehlinger, A., Randles, L., Lary, J. W., Kang, Y., Haririnia, A., Storaska, A. J., Cole, J. L., Fushman, D., and Walters, K. J. (2009) Structure of the s5a:k48-linked diubiquitin complex and its interactions with rpn13. *Mol. Cell 35*, 280–290.
86. Dickinson, B. C., Varadan, R., and Fushman, D. (2007) Effects of cyclization on conformational dynamics and binding properties of Lys48-linked di-ubiquitin. *Protein Sci. 16*, 369–378.
87. Davies, B. A., Lee, J. R., Oestreich, A. J., and Katzmann, D. J. (2009) Membrane protein targeting to the MVB/lysosome. *Chem. Rev. 109*, 1575–1586.
88. Sims, J. J., and Cohen, R. E. (2009) Linkage-specific avidity defines the lysine 63-linked polyubiquitin-binding preference of rap80. *Mol. Cell 33*, 775–783.
89. Cook, W. J., Jeffrey, L. C., Carson, M., Chen, Z., and Pickart, C. M. (1992) Structure of a diubiquitin conjugate and a model for interaction with ubiquitin conjugating enzyme (E2). *J. Biol. Chem. 267*, 16467–16471.